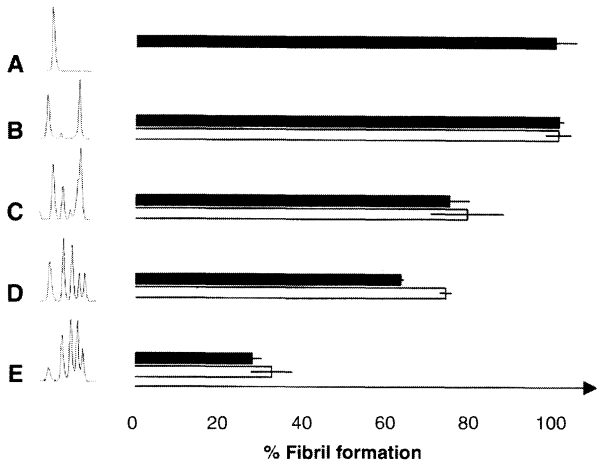

Fig. 4. Fibril formation as a function of the extent of hybrid tetramer formation. Chromatograms from analytical anion exchange chromatography quantifying the amount of subunit exchange are shown on the left and the extent of fibril formation represented by bar graphs (turbidity at 400 nm) on the right. (**A**) The extent of amyloidogenicity from the V30M homotetramer **1** [0.2 mg/ml (pH 4.4); 37 °C; 72 hours; set to 100%]. Entry (**B**) displays the amyloidogenicity arising from mixing homotetramers **1** and **5** (open bar) and **1** (filled bar) with an untagged T119M homotetramer immediately before triggering fibril formation by lowering the pH. No suppression of V30M amyloidogenicity occurs, due to lack of subunit exchange. (**C**) When tetramer **1** and the T119M homotetramer (filled bar) or tetramers **1** and **5** (open bar) are preincubated at 4°C for 18 days (*20*) some exchange occurs, consistent with the modest suppression of amyloidogenicity. (**D**) The unfolding/refolding protocol (*26*) provides assembly-competent monomeric T119M suppressor subunits which exchange with subunits in V30M homotetramer **1** after 24 hours (4°C). The amyloidogenicity of the tetramers resulting from exchange between native V30M and monomeric T119M (filled bar) or FT_2-T119M (open bar) is shown. (**E**) Amyloid formation from co-reconstituted TTR [V30M and T119M (filled bar) or FT_2-T119M (open bar)] as described in (*20*), affording a near-statistical distribution of tetramers (1:4:6:4:1), exhibited a 70% inhibition of amyloid formation.

rapid dilution of equimolar concentrations (to 0.05 mg/ml) of unfolded V30M and FT_2-T119M or T119M subunits (in 6.5 M GdmCl preincubated for 48 hours at 4°C) at 25°C. The refolded protein was purified by dialysis and gel filtration (Superdex 75, Pharmacia).

21. F. E. Dwulet, M. D. Benson, *Proc. Natl. Acad. Sci. U.S.A.* **81**, 694 (1984).
22. M. J. M. Saraiva, S. Birken, P. P. Costa, D. S. Goodman, *J. Clin. Invest.* **74**, 104 (1984).
23. Y. Ando *et al.*, *Amyloid* **6**, 119 (1999).
24. By extension, the impotency of the WT subunit as a suppressor predicts that the fibrils in heterozygous patients (V30M/WT) formed in tissues imposing a strong denaturation stress will be composed of both V30M and WT subunits, because all five tetramers would be amyloidogenic. The 1:1 ratio of V30M and WT subunits composing cardiac amyloid deposits seems to verify this prediction (*27*). In other tissues, however, such as in the kidney (*21, 22*) and the vitreous body (*23*), the bias toward V30M subunits composing the deposits is evident, suggesting that the denaturation stress in these tissues is not as severe; therefore, only tetramer **1** and V30M-rich tetramers **6** and **7** serve as precursors as opposed to the WT-rich tetramers **8** and **9**, which are more stable, at least toward chaotrope denaturation (Fig. 3B) (*10*).
25. O. B. Suhr *et al.*, *Transplantation* **60**, 933 (1995).
26. Proof of principle that it is possible to include T119M supressor subunits into a TTR tetramer after secretion was demonstrated by adding folded T119M monomers to V30M homotetramer **1** undergoing subunit exchange at 4°C. A folded T119M or FT_2-T119M monomer was produced by first unfolding the tetramer in 6.5 M guanidinium chloride (GdmCl) at 4°C (48 hours) and then refolding it by rapid dilution. The monomer resists self-tetramerization at 4°C, allowing it to be mixed with tetramer **1** (4°C), which by subunit exchange incorporates T119M subunits and resists acid-induced fibril formation (Fig. 4D). A detailed procedure is available (*10*). Further elaboration will be required to achieve this result by intravenous administration of T119M TTR monomers.
27. M. Yazaki *et al.*, *Biochem. Biophys. Res. Commun.* **274**, 702 (2000).
28. TTR (1 μM monomer concentration) was prepared in GdmSCN (0 to 3 M) and incubated for 24 hours (25°C) in buffer [50 mM phosphate buffer (pH 7.0) with 1 mM EDTA and 1 mM dithiothreitol added]. Denaturation curves were generated by the ratio of the tryptophan fluorescence intensity [355 nm (unfolded maximum)]/[335 nm (folded maximum)]; excitation is at 295 nm. The unfolding data were normalized from linear baseline dependence on denaturant and fitted to a two-state unfolding transition as described (*13*). Estimates of $\Delta G_{NU} = -RT\ln [D]/[N]$ were calculated assuming a linear dependence of ΔG on denaturant concentration using $\Delta G_{NU} = \Delta G_{NU}{}^{H_2O} - m[GdmSCN]$.
29. We thank G. Dendle for help with protein expression and purification, H. Purkey for assistance with the T4 binding assay, J. White for RBP binding measurements, S. Deechongkit and H. M. Petrassi for help with analytical ultracentrifugation, and A. Sawkar for assistance with the unfolding refolding protocol. We are also grateful to J. Buxbaum for fruitful discussions regarding the clinical aspects and R. Lerner for critical comments on the manuscript. Supported by a grant from NIH (DK46335-09), The Skaggs Institute of Chemical Biology, The Lita Annenberg Hazen Foundation, and a postdoctoral fellowship to P.H. from The Wenner-Gren Foundations.

3 May 2001; accepted 3 August 2001

Strand-Specific Postreplicative Processing of Mammalian Telomeres

S. M. Bailey,[1] M. N. Cornforth,[2] A. Kurimasa,[3] D. J. Chen,[3] E. H. Goodwin[1]*

Telomeres are specialized nucleoprotein structures that stabilize the ends of linear eukaryotic chromosomes. In mammalian cells, abrogation of telomeric repeat binding factor TRF2 or DNA-dependent protein kinase (DNA-PK) activity causes end-to-end chromosomal fusion, thus establishing an essential role for these proteins in telomere function. Here we show that TRF2-mediated end-capping occurs after telomere replication. The postreplicative requirement for TRF2 and DNA-PKcs, the catalytic subunit of DNA-PK, is confined to only half of the telomeres, namely, those that were produced by leading-strand DNA synthesis. These results demonstrate a crucial difference in postreplicative processing of telomeres that is linked to their mode of replication.

Telomeres are nucleoprotein structures at the ends of chromosomes that are composed of repetitive G-rich sequence (TTAGGG in vertebrates) and a variety of associated telomeric binding proteins. Together, they form a dynamic terminal structure that "caps" the natural ends of linear chromosomes (*1*, *2*). This cap prevents degradation of chromosome ends and protects against inappropriate recombination. TRF2 (*3*, *4*) and the three subunits of DNA-PK—Ku70, Ku80, and the catalytic subunit DNA-PKcs (*5*–*8*)—are among the proteins that participate directly in capping mammalian chromosomes. Direct visualization of mammalian telomeres by electron microscopy has revealed the existence of terminal structures known as t loops (*9*), which are created when a telomere end loops back on itself and invades an interior segment of duplex telomeric DNA. By sequestering natural chromosome ends, t loops may render telomeres nonrecombinogenic. It has been proposed that formation of t loops is mediated by TRF1 and TRF2 and requires a single-stranded extension of the TTAGGG sequence

[1]Bioscience Division, Los Alamos National Laboratory, Los Alamos, NM 87544, USA. [2]Department of Radiation Oncology, University of Texas Medical Branch, Galveston, TX 77550, USA. [3]Cell and Molecular Biology Division, Lawrence Berkeley National Laboratory, Berkeley, CA 94720, USA.

*To whom correspondence should be addressed. E-mail: egoodwin@telomere.lanl.gov

(*10*). However, other mechanisms of end-capping cannot be formally excluded, particularly in light of the controversy over whether all telomeres have 3′ overhangs suitable for t loop formation (*11*, *12*).

To investigate the capping mechanism, we used a dominant-negative mutant of TRF2, TRF2$^{\Delta B \Delta M}$, that lacks both the NH_2-terminal basic domain and the COOH-terminal Myb domain. TRF2$^{\Delta B \Delta M}$ removes endogenous TRF2 from telomeres, resulting in diminished 3′ overhangs, induction of end-to-end fusions, formation of anaphase bridges, activation of DNA damage checkpoints, and impaired cell growth (*3*, *4*). The uncapped telomeres are presumably "repaired" by nonhomologous end-joining (NHEJ), resulting in covalent end-to-end ligations that preserve telomeric DNA at the point of fusion.

We expressed TRF2$^{\Delta B \Delta M}$ for 5 days in two independent clones of HTC75 human fibrosarcoma cells (*13*). Microscopic examination revealed that 44 of 154 mitotic cells exhibited end-to-end chromosomal fusions (*14*). In those cells containing fusions, the average frequency was 3.1 per cell. All were chromatid-type fusions involving at least two (and frequently multiple) chromosomes joined together end to end. This type of aberration, which we designate as telomeric chromatid concatenates (TCCs), is noteworthy because it demonstrates that this type of telomeric fusion can form only after replication of telomeric DNA (fusions in G_1 produce chromosome-type aberrations). The exclusive appearance of TCCs suggests that telomere replication is a prerequisite for fusion; i.e., TRF2-mediated end-capping follows telomere replication. The absence of chromosome-type telomeric fusions also indicates that cells with TCCs do not progress through a second cell cycle. This is perhaps not surprising because anaphase bridging—the inevitable result of the numerous dicentric chromosomes created by telomeric fusion—would be expected to impede cell division.

These observations focused our attention on the role of DNA replication in end-capping. Telomeres face special challenges during replication. The protective terminal structure of the telomere must not only disassemble in order to replicate, it must also regenerate after replication. The two telomeres at the end of each mitotic chromosome arm replicate from a single parental telomere. One is produced through leading-strand DNA synthesis, the other through lagging-strand synthesis, hereafter referred to as the leading-strand and the lagging-strand telomeres, respectively. Immediately after replication, leading-strand telomeres are blunt ended and lagging-strand telomeres have a short 3′ G-rich single-stranded overhang. Both types of ends may be processed further, perhaps by C-rich strand degradation and/or sequence addition by telomerase (*11*, *15*, *16*).

Because sister telomeres remain in close proximity during interphase, one might expect that impaired end-capping would lead to a preponderance of telomeric fusions between sister chromatids. However, out of the 135 fusions observed, none resulted from sister union. This finding is noteworthy because it indicates that, of the two telomeres replicated from the same template, only one acquires the ability to fuse to other telomeres in the presence of TRF2$^{\Delta B \Delta M}$.

To differentiate leading-strand from lagging-strand telomeres (Fig. 1), we used a procedure based on the strand-specific in situ hybridization technique of chromosome-orientation fluorescence in situ hybridization (CO-FISH) (*17*). Unique hybridization patterns are produced for each of the three possible types of chromatid telomeric fusions: leading-to-leading strand, leading-to-lagging strand, and lagging-to-lagging strand (Fig. 1D). Using this strategy, we sought to determine whether impaired end-capping is limited to telomeres synthesized by one mode of replication or, alternatively, whether fusion is random but exclusive. In the latter case, either a leading-strand or a lagging-strand telomere might engage in fusion, thereby preventing its sister telomere from doing the same. These experiments (*18*) revealed that TCCs were overwhelmingly the products of fusion between leading-strand telomeres (Fig. 2). If mere chance dictates the type of fusion, the expected ratio of fusion products depicted in Fig. 2 would be 1:2:1. Instead, 133 out of 135 observed fusions had a pattern consistent with

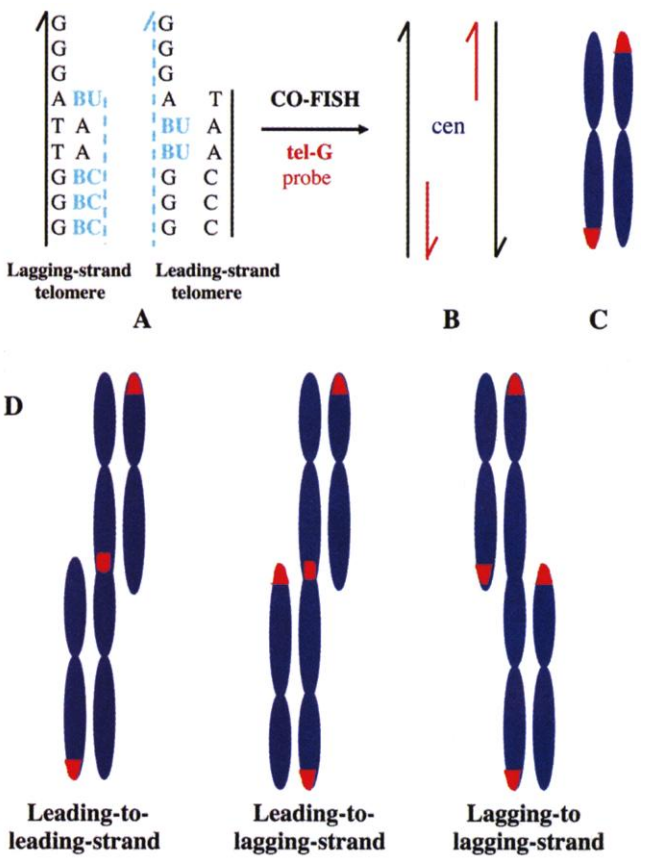

Fig. 1. Identification of leading-strand and lagging-strand telomeres. (**A**) Cells expressing TRF2$^{\Delta B \Delta M}$ are allowed to replicate their DNA once in the presence of bromodeoxyuridine (BU) and bromodeoxycytidine (BC) and are then collected in mitosis. Because DNA synthesis is semiconservative, opposite strands of the telomere sequence are bromo-substituted. Each mitotic chromosome has one parental DNA strand and one newly synthesized bromo-substituted strand. After the cells are fixed and dropped onto microscope slides, the bromo-substituted strands are degraded by sequential UV and exonuclease treatments. (**B**) Each sister chromatid of a mitotic chromosome now contains just one of the parental DNA strands. A labeled $(TTAGGG)_7$ single-stranded probe hybridizes to those telomeres that were replicated by leading-strand synthesis. Likewise, a $(CCCTAA)_7$ probe would hybridize and identify lagging-strand telomeres. (**C**) Viewed by fluorescence microscopy, mitotic chromosomes have two telomere signals (red) in contrast to the four signals observed with ordinary FISH. (**D**) Each of the three different types of TCCs can be identified by its unique hybridization pattern. Shown here are the patterns expected for the $(TTAGGG)_7$ probe.

Table 1. Number of telomeric chromatid concatenates (TCCs) in HTC75 cells.

Clone	Leading-Leading	Leading-Lagging	Lagging-Lagging
T:22			
Total*	95	0	1
Complete†	70	0	0
T:19			
Total	38	0	1
Complete	36	0	0

*Analysis of all TCCs observed. †Analysis of TCCs with a complete complement of hybridization signals.

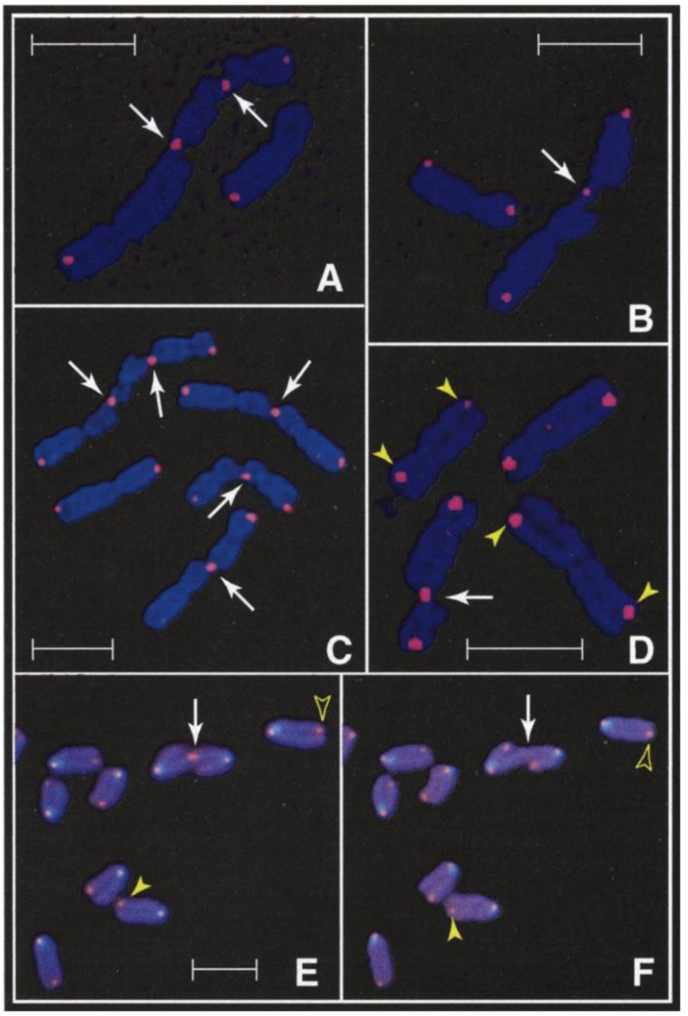

Fig. 2. Images of partial metaphases with several TCCs as detected by CO-FISH. Telomeric DNA is detected with Cy3 (red), and chromosomal DNA is counterstained with DAPI (blue). (**A** to **D**) Fusion points of several concatenates in human HTC75 cells induced by the truncated TRF2$^{\Delta B \Delta M}$ protein are identified by white arrows. At the point of joining, only one chromatid from each of the two participating chromosomes enters into the fusion. All TCCs involve only leading-strand telomeres (identified by the G-rich telomere probe). (D) The top chromosome identified by yellow arrowheads has two leading-strand telomeres on the same chromatid. This "cis" configuration is the result of one (or any odd number) sister chromatid exchange, which are common events particularly in subtelomeric regions (*23*). The lower chromosome with yellow arrowheads displays the "trans" configuration. (**E** and **F**) Analysis of a mouse *scid* (DNA-PKcs–deficient) cell containing a telomeric chromatid fusion. (E) The G-rich probe identifies it as a leading-leading strand fusion. (F) The same cell after removal of the G-rich probe by denaturation and hybridization of the C-rich probe. A reciprocal pattern, as indicated by arrowheads at the point of fusion and at the ends of two chromosomes, is obtained and illustrates the exquisite strand specificity of the technique. The light blue fluorescence in centromeric regions is due to "lateral asymmetry" [see (*24*)]. Scale bars, 5 μm.

fusion between two leading-strand telomeres, and none were of the leading-to-lagging strand type (Table 1). Two fusions were tentatively identified as lagging-to-lagging strand types, because they lacked hybridization signal at the point of fusion. However, because they also lacked one or more hybridization signals at other telomere sites, these could not be definitively classified. When analysis was restricted to the 106 fusion events displaying a full complement of hybridization signals, all were the result of leading-to-leading strand fusion. For a random process, only one-fourth of all fusions should be of this type; therefore, the difference from expectation is highly significant (χ^2 test, $P \ll 0.001$).

TCCs also occur in cells with reduced DNA-PK activity, although they are far less frequent and produce a much milder phenotype. Inspection of 850 DNA-PKcs–deficient mouse fibroblasts (*13*) identified only 14 such chromatid-type events (Table 2). CO-FISH analysis revealed that all 14 were of the leading-to-leading strand variety. Again, this proportion differs significantly from that expected of random end-to-end fusion ($P < 0.001$). In contrast, no telomeric fusions were seen in 800 wild-type repair-proficient mouse fibroblasts.

Conceivably, end-capping failure may affect only leading-strand telomeres because they have an absolute requirement for TRF2 and DNA-PKcs to refashion their blunt ends after replication. Lagging-strand telomeres already have 3′ overhangs after replication, so postreplicative processing may not be essential (but could occur to some extent). Both telomeres may then be folded into t loops as their final configuration. This interpretation is appealing for DNA-PKcs because of its role in DNA repair, which requires end processing. However, TRF2 is more commonly

Table 2. TCCs in five DNA-PK–deficient mouse cell lines.

Cell type	Number of cells scored	Number of leading-leading TCCs
scid, primary	200	3
DNA-PK$^{-/-}$, primary	100	1
scid, transformed	200	5
DNA-PK$^{-/-}$, transformed	100	3
p53$^{-/-}$/*scid*, transformed	250	2

associated with remodeling chromosome ends into t loops (*9*, *10*). If TRF2's role is confined to t loop formation, it would be difficult to explain the lack of lagging-strand telomeric fusions in cells expressing TRF2$^{\Delta B \Delta M}$. Alternatively, there may be essential differences in capping leading- and lagging-strand telomeres beyond remodeling ends into 3′ overhangs. At present, neither interpretation can be excluded.

The indispensable role played by chromosomal termini in maintaining the stable inheritance of genetic information is underscored by the severity of the phenotype associated with dysfunctional telomeres. Curiously, telomere dysfunction has itself opened a window into understanding these essential structures.

References and Notes

1. E. H. Blackburn, J. W. Szostak, *Annu. Rev. Biochem.* **53**, 163 (1984).
2. V. A. Zakian, *Annu. Rev. Genet.* **23**, 579 (1989).
3. B. van Steensel, A. Smogorzewska, T. de Lange, *Cell* **92**, 401 (1998).
4. J. Karlseder, D. Broccoli, Y. Dai, S. Hardy, T. de Lange, *Science* **283**, 1321 (1999).
5. S. M. Bailey *et al.*, *Proc. Natl. Acad. Sci. U.S.A.* **96**, 14899 (1999).
6. H. L. Hsu, D. Gilley, E. H. Blackburn, D. J. Chen, *Proc. Natl. Acad. Sci. U.S.A.* **96**, 12454 (1999).
7. E. Samper, F. A. Goytisolo, P. Slijepcevic, P. P. W. van Buul, M. A. Blasco, *EMBO Rep.* **1**, 244 (2000).
8. F. A. Goytisolo, E. Samper, S. Edmonson, G. E. Taccioli, M. A. Blasco, *Mol. Cell. Biol.* **21**, 3642 (2001).
9. J. D. Griffith *et al.*, *Cell* **97**, 503 (1999).
10. A. Smogorzewska *et al.*, *Mol. Cell. Biol.* **20**, 1659 (2000).
11. V. L. Makarov, Y. Hirose, J. P. Langmore, *Cell* **88**, 657 (1997).
12. W. E. Wright, V. M. Tesmer, K. E. Huffman, S. D. Levene, J. W. Shay, *Genes Dev.* **11**, 2801 (1997).
13. Production and maintenance of the HTC75 human fibrosarcoma cell lines containing a TRF2 dominant-negative allele under control of a doxycycline-repressible promoter were described previously (*3*), as were the mouse scid and p53$^{-/-}$/scid cell lines (*5*) and DNA-PK$^{-/-}$ cells (*19*).
14. Metaphase spreads were prepared by standard techniques as described in (*5*).
15. R. J. Wellinger, K. Ethier, P. Labrecque, V. A. Zakian, *Cell* **85**, 423 (1996).
16. T. R. Cech, *Angew. Chem. Int. Ed.* **39**, 34 (2000).
17. CO-FISH, previously described in detail (*20*, *21*), was used here with some modification. Briefly, confluent cell monolayers were subcultured into medium containing a 3:1 ratio of 5′-bromo-2′-deoxyuridine (BrdU):5′-bromo-2′-deoxycytidine (BrdC) (Sigma) at a total final concentration of 1×10^{-5} M for 24 hours, with Colcemid (0.2 μg/ml) being added for the final 4 hours. Cultures were harvested and metaphase spreads were prepared

on microscope slides, which were then treated with ribonuclease A (0.5 mg/ml) for 10 min at 37°C. Chromosomal DNA was stained with Hoechst 33258 (0.5 μg/ml; Sigma) in 2× standard saline citrate (SSC) for 15 min at room temperature. Slides were then exposed to 365-nm ultraviolet (UV) light (Stratalinker 1800 UV irradiator) for 25 to 30 min. The BrdU/BrdC-substituted DNA was digested with Exonuclease III (3 U/μl; Promega) in 50 mM tris-HCl (pH 8.0), 5 mM $MgCl_2$, and 5 mM dithiothreitol for 10 min at room temperature. Chromosomes were briefly denaturated in 70% formamide, 2× SSC at 70°C (1 min) and then dehydrated through a cold ethanol series (70%, 85%, and 100%). A $(TTAGGG)_7$ probe was synthesized, labeled with Cy3 as in (*22*), and hybridized to the now single-stranded chromosomal target DNA, as in (*5*). Chromosomes were counterstained with the blue-fluorescing dye 4′,6-diamidino-2-phenylindole (DAPI).

18. To be scored as a telomeric fusion, the DAPI signal had to be continuous through the point of fusion, with the two telomeres fused into a single FISH signal. The results of hybridization analysis of HTC75 clones were confirmed in two independent laboratories. Mitotic spreads were examined with Zeiss Axiophot microscopes equipped for epifluorescence, with either a 100-watt high-pressure mercury (OSRAM) or a 75-watt mercury-xenon light source (Hamamatsu). DAPI and Cy3 exicitor/dichroic/barrier filter sets (Omega Optical) were used to detect counterstained chromosomes and telomere signals, respectively. For mouse chromosomes, which tend to have large (bright) telomeres, fluorescent specimens were observed directly through the oculars of the microscope. Digital images of human chromosomes were captured with a SensSys A2S black and white charge-coupled device video camera (Photometrics), controlled by an Apple G3 computer, running Powergene MacProbe analysis software (Applied Imaging). DAPI and Cy3 channels were pseudocolored (blue and red, respectively) before being merged to produce the images shown.
19. A. H. Kurimasa *et al.*, *Proc. Natl. Acad. Sci. U.S.A.* **96**, 1403 (1999).
20. E. H. Goodwin, J. Meyne, S. M. Bailey, *Cytogenet. Cell Genet.* **63**, 253 (1993).
21. S. M. Bailey, J. Meyne, E. H. Goodwin, in *DNA Damage and Repair*, J. Nickoloff, M. Hoekstra, Eds. (Humana Press, Totowa, NJ, 2001), vol. 3, chap. 14.
22. J. Meyne, E. H. Goodwin, *Chromosome Res.* **3**, 375 (1995).
23. M. N. Cornforth, R. L. Eberle, *Mutagenesis* **16**, 85 (2001).
24. E. H. Goodwin, J. Meyne, S. M. Bailey, D. Quigley, *Chromosoma* **104**, 345 (1996).
25. We thank T. de Lange for the HTC75 cell lines and R. Eberle for expert technical assistance. Supported by grants from the Department of Energy/Office of Biological and Energy Research (W-7405-ENG-36, ER62684, and DEAC03-76SF00098), the National Cancer Institute (CA76260), the U.S. Army (DAMD17-97-1-7165), and NIH (AG-917709 and CA50519).

8 May 2001; accepted 3 August 2001

Dendrodendritic Inhibition Through Reversal of Dopamine Transport

Björn H. Falkenburger, Karen L. Barstow, Isabelle M. Mintz*

Synapses in the central nervous system are usually defined by presynaptic exocytotic release sites and postsynaptic differentiations. We report here a demonstration of dendrodendritic inhibition that does not engage a conventional synapse. Using amperometric and patch-clamp recordings in rat brain slices of the substantia nigra, we found that blockade of the dopamine transporter abolished the dendritic release of dopamine and the resulting self-inhibition. These findings demonstrate that dendrodendritic autoinhibition entails the carrier-mediated release of dopamine rather than conventional exocytosis. This suggests that some widely used antidepressants that inhibit the dopamine transporter may benefit patients in the early stages of Parkinson's disease.

Dopaminergic neurons of the substantia nigra are important modulators of basal ganglia function. Their degeneration leads to severe motor and cognitive deficits in Parkinson's disease (*1, 2*). They exert their influence distally, in the striatum, globus pallidum, and subthalamus (*3*), through the release of dopamine at axon terminals, and locally, in the substantia nigra, through the dendritic release of dopamine (*4–6*). Because dopamine hyperpolarizes dopaminergic neurons (*7*), it is widely accepted that the dendritic release of dopamine primarily leads to the autoinhibition of dopaminergic neurons (*8*), yet this has never been shown. Dopamine efflux has been documented in dendrites stimulated by high K concentrations (*4, 9, 10*), glutamate (*11*), amphetamine (*10*), and large electrical fields (*12*), and the molecular steps coupling dopamine autoreceptor activation to inhibition have also been identified (*7*). Inhibitory postsynaptic potentials (IPSPs) indicating a physiological response to released dopamine have not been seen in the substantia nigra.

We addressed this issue with patch-clamp and amperometric recording methods (*13*). To trigger release by a large population of dendrites, we chose to stimulate the subthalamic nucleus, because its neurons provide a robust glutamatergic input to nigral dopaminergic cells (*14*), and its activation in vivo increases extracellular dopamine in the substantia nigra (*15, 16*).

Subthalamic neurons can be stimulated in vitro to produce measurable release of dopamine in the substantia nigra (Fig. 1A). Amperometric recordings in the pars reticulata revealed that subthalamic stimulation elicited small but reproducible current transients (2.3 ± 0.7 pA, n = 14), indicating an increase in extracellular dopamine of about 15 to 20 nM (*17*). These transients showed greater amplitude in the pars reticulata, consistent with the large number of subthalamic terminals reported in this region (*7*).

To study the postsynaptic effects of released dopamine, we selected a subset of dopaminergic neurons whose cell bodies, located in the pars reticulata (*3*), may lie close to releasing dendrites (Fig. 1B, cell B in upper panel). These neurons were identified by their characteristic firing properties, morphology, or positive labeling by antibodies to tyrosine hydroxylase (*13*). In control conditions, they responded to repetitive subthalamic stimulation with summating monosynaptic excitatory postsynaptic potentials (EPSPs) that were followed by a slow, delayed hyperpolarization (Fig. 1B, lower panel, n = 152/173). This hyperpolarization reached a peak amplitude of 6.2 ± 3.0 mV (mean ± SEM, n = 51). It was reduced by the D2 receptor antagonist sulpiride (on average by 73.3 ± 15.1%, n = 15). Hence, for a small contingent of dopaminergic neurons, these findings establish a clear and reliable IPSP in response to dendritically released dopamine.

Dopaminergic neurons of the pars compacta never displayed such IPSPs in control conditions (Fig. 1C, left panel). We assumed that this apparent lack of response to dopamine might reflect the bias of our recording conditions, which favor detection of somatic synaptic potentials and actively amplified dendritic EPSPs over that of remote IPSPs that attenuate through passive propagation. Consistent with this hypothesis, in every tested cell, the inhibitory response to released dopamine was uncovered after partial blockade of the subthalamic EPSP with the glutamate receptor antagonists D(-)-2-amino-5-phosphonopentanoic acid (D-AP5, 50 μM) and 6-cyano-7-nitroquinoxaline-2,3-dione (CNQX, 5 μM) (Fig. 1C, left panel, n = 21). These

Department of Pharmacology and Experimental Therapeutics, Boston University Medical Center, Boston, MA 02118, USA.

*To whom correspondence should be addressed. E-mail: imintz@bu.edu